Reducing Logprob Without Causal Verification: Diagnosing SAE-Based PII Suppression in LLMs

Anonymous ACL submission

Abstract

SAE-based feature-level interventions to suppress PII leakage in LLMs are primarily evaluated by log-probability reduction. We show that this criterion cannot distinguish feature-specific suppression from a magnitude artifact: a direction-agnostic effect of sufficiently large activation perturbations. Across 36 (model, layer, PII type) cases, we compare selected SAE feature interventions with coherence-matched random direction controls using logprob and rank-aware metrics. While 17 cases (47%) appear successful under logprob-only evaluation, only 1 case (2.8%) passes our multi-metric framework. The rest reveal two failure modes: random directions outperform selected features, and feature selection collapse across PII types. These results indicate that existing evaluations cannot verify whether interventions target causal pathways of PII leakage, and we propose a new research mission: causally grounded PII suppression through circuit-level localization and causal mediation analysis.

1 Introduction

Large Language Models (LLMs) are increasingly being deployed in domains that handle sensitive information, such as healthcare, law, and finance (Chen et al., 2024b). However, during pretraining, LLMs can memorize Personally Identifiable Information (PII) contained in their training data, which may subsequently be exposed when the model is prompted with a crafted prefix (Carlini et al., 2021, 2023). PII leakage has therefore emerged as a critical security and ethical concern.

Recent work has attempted to mitigate PII leakage by applying Sparse Autoencoders (SAEs) to LLM activations, identifying features hypothesized to encode PII, and intervening on them through feature ablation or vector steering (Frikha et al., 2025). Following common practice in PII leakage research, these studies evaluate intervention success via reductions in PII-token log-probability (Kim et al., 2023; Nakka et al., 2024). However, this metric cannot distinguish feature-specific suppression from a magnitude artifact—a generic effect of sufficiently large perturbations regardless of direction. Whether such reductions reflect interventions on PII-specific features or generic activation perturbations therefore remains unverified, motivating our study.

To empirically examine this limitation, we conduct a selectivity experiment comparing interventions along putatively PII-related SAE feature directions with interventions along coherence-matched random directions. Our results show no statistically significant differences between the two interventions across logprob and rank metrics, suggesting that existing evaluations fail to distinguish feature-specific effects from generic activation perturbations. This concern is compounded by growing evidence that SAE feature directions may not be reliably distinguishable from random baselines in general settings (Korznikov et al., 2026; Ronge et al., 2026); our findings instantiate this general critique in the concrete setting of PII suppression.

These findings call for a fundamental reassessment of existing SAE-based PII suppression methods. We propose a new research mission for NLP: identifying the causal pathways of PII leakage and developing interventions grounded in them, moving beyond correlational feature-level suppression toward causally grounded approaches.

The contributions of this paper are as follows.

- We empirically demonstrate, using coherence-matched random direction controls and a rank-based metric, that log-probability-based evaluations fail to verify feature-specificity of SAE-based PII suppression interventions across 36 experimental configurations.
- We propose a causal research agenda for PII suppression, calling for interventions grounded in identified causal pathways rather than correlational feature associations.

2 SAE-based PII Suppression in LLMs

Recent work on PII suppression has shifted from neuron-level interventions (Chen et al., 2024a) to SAE-based feature-level interventions (Frikha et al., 2025) that ablate or steer features assumed to encode PII, evaluated primarily by log-probability reduction. However, this metric cannot distinguish feature-specific suppression from a magnitude artifact—a direction-agnostic effect of any sufficiently large hidden-state perturbation—and cannot verify whether reductions reflect interventions on PII-specific causal mechanisms. This concern is compounded by growing evidence that SAE feature directions may not be reliably distinguishable from random baselines (Korznikov et al., 2026; Ronge et al., 2026), motivating our selectivity experiment comparing selected feature interventions against coherence-matched random direction controls (additional background in Appendix A.1).

3 Experimental Setup

Models and data. We evaluate SAE-based PII suppression on three general-purpose LLMs: two 8B-class models (Llama-3.1-8B-Instruct (Grattafiori et al., 2024) and Qwen3-8B (Yang et al., 2025)) and one 9B-class model (Gemma-2-9B (Gemma Team, 2024)), all LoRA (Hu et al., 2022) fine-tuned on the same synthetic medical PII corpus. Each example appends four PII fields (name, patient ID, phone number, and email) to the end of a clinical note. We use the medical domain because PII memorization in clinical LLMs is a well-documented privacy concern (Lehman et al., 2021), and synthetic data lets us study it without exposing real patient information. Feature discovery and final evaluation are performed on mutually disjoint PII-pair splits. Task-specific SAEs are trained on a separate 50k synthetic clinical note corpus with no entity-level overlap with either the LLM fine-tuning corpus or the evaluation pairs, so the SAEs learn general representation patterns of PII rather than memorizing specific PII entities.

Task-specific SAEs and feature discovery. For each model, we train task-specific top-k SAEs (Gao et al., 2025) at three depth-proportional layers, approximately corresponding to 25%, 50%, and 75% of the model depth (expansion factor $\times 8$, sparsity $k = 32$). This depth-proportional sampling is a pre-specified design choice following prior findings that linguistic and semantic representations vary across depth (Tenney et al., 2019; Jawahar et al., 2019; Jin et al., 2025). For each (model, layer, PII type), we identify high-activation non-dead SAE features near the PII marker as candidates and designate as the selected feature the one that yields the largest reduction in gold PII span logprob on the discovery split. This logprob-driven selection mirrors the standard approach in existing SAE-based PII suppression work that we evaluate; our contribution is to diagnose how such selected features behave under metrics beyond logprob and under random-direction controls.

Hidden-space intervention and random control. We use a hidden-space intervention that directly modifies the LLM hidden state along the decoder direction of a selected SAE feature. At token position t in layer ℓ:

$$h'_t = h_t + \alpha \cdot z_t[f] \cdot W_{\text{dec}}[f],$$

where $z_t[f]$ is the SAE activation of selected feature f and $W_{\text{dec}}[f]$ is its decoder direction. We fix $\alpha = -2$ (sensitivity in Appendix A.11). Under a linear decoder, this is equivalent to a z-space edit up to a reconstruction-error term that cancels in the selectivity ratio (Table 4). Due to top-k sparsity, the intervention term automatically vanishes at positions where $z_t[f] = 0$, so the intervention only acts where the selected feature is active without requiring an explicit PII-span mask. To distinguish feature-specific intervention from generic magnitude perturbation, we use a coherence-matched random control that preserves the token-wise magnitude $m_t = \|z_t[f] \cdot W_{\text{dec}}[f]\|_2$ but replaces only the direction with an isotropic random unit vector r: $h'_t = h_t + \alpha \cdot m_t \cdot r$. The same r is shared across all intervened positions within a forward pass, matching the span-level direction coherence of the selected-feature intervention. Random-control results are averaged over three independent seeds.

Evaluation metrics. We define a cell as one (model, layer, PII type) combination and evaluate each intervention with two signed metrics: (i) Δ_{lp}, the change in the mean log-probability of the gold PII span ($\Delta_{\text{lp}} < 0$ indicates reduced leakage), and (ii) Δ_{br}, the change in a rank-aware extraction-cost proxy $b_{\text{rank}}(y) = \sum_{t \in y} \log_2(\text{rank}_t)$ ($\Delta_{\text{br}} > 0$ indicates that gold PII tokens move backward in the candidate ranking and become harder to extract). Selectivity is defined as the effect-magnitude ratio between the selected feature and the random

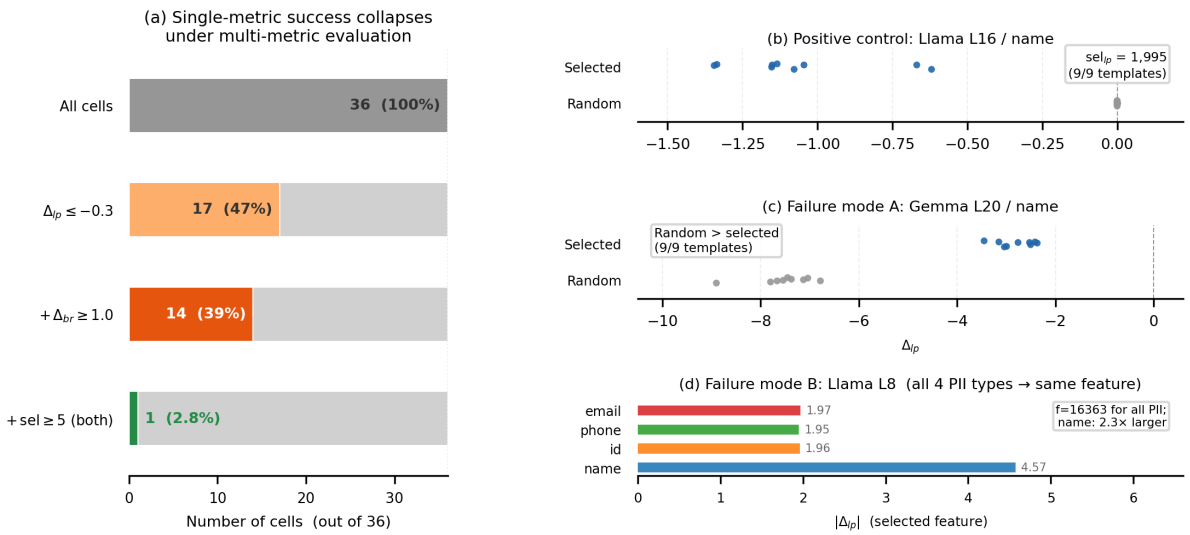

Figure 1: Main diagnostic results across 36 (model, layer, PII type) cells. (a) Number of cells passing single-metric vs. multi-metric criteria. (b, c) Per-template Δ_{lp} for selected feature vs. coherence-matched random control. (d) $|\Delta_{lp}|$ per PII type in Llama L8, where f=16363 is selected for all four types.

control: $\mathrm{Sel}_{\mathrm{lp}} = |\Delta_{\mathrm{lp}}^{\mathrm{target}}|/|\Delta_{\mathrm{lp}}^{\mathrm{random}}|$, and $\mathrm{Sel}_{\mathrm{br}}$ is defined analogously. We call a cell clean-strong if it satisfies all four conjunctive criteria: $\Delta_{\mathrm{lp}} \leq -0.3$, $\Delta_{\mathrm{br}} \geq +1.0$, $\mathrm{Sel}_{\mathrm{lp}} \geq 5$, and $\mathrm{Sel}_{\mathrm{br}} \geq 5$. Evaluation is performed across nine prompt templates (T0: the 4-PII training format; T1–T8: isolated target PII with varying label formats including Korean, JSON, and narrative forms), and each cell-level value is averaged over 50 pairs $\times$ 9 templates $=$ 450 evaluation contexts. Detailed hyperparameters, the full prompt template list, and exact definitions of category labels (clean-weak, anti-suppression, inactive, etc.) are provided in Appendix A.2 and A.4.

4 Results

Across 36 cells, only one satisfies our multi-metric criterion. The remaining cells exhibit two (non-exclusive) failure modes detailed below: Failure mode A (random-dominant) and Failure mode B (feature selection collapse). Figure 1 summarizes the main findings, and full 36-cell results are reported in Appendix A.5.

Single-metric evaluation overestimates suppression. A logprob-only criterion ($\Delta_{\mathrm{lp}} \leq -0.3$) labels 17/36 cells (47%) as apparent PII suppression candidates. However, when we apply the four conjunctive criteria that jointly require a rank-aware metric and coherence-matched random-control selectivity, only one cell remains clean-strong (1/36, 2.8%; Llama L16/name; Figure 1a). This conclusion is robust to the selectivity threshold: relaxing it to ≥ 2 leaves only 3/36 cells (8.3%), while tightening it to ≥ 10 still leaves the same single cell (Appendix A.10).

Positive control: Llama L16/name. Llama L16/name, the only clean-strong configuration, serves as a positive control showing that our criterion is not impossibly strict (Figure 1b). It satisfies the criterion across all nine templates, maintaining $\mathrm{Sel}_{\mathrm{lp}} > 400$ even on Korean (T5) and JSON (T7) formats that differ substantially from the training format T0. The cell mean reaches $\mathrm{Sel}_{\mathrm{lp}} \approx 1{,}995$, with random-control $|\Delta_{\mathrm{lp}}|$ near the measurement floor ($\approx 10^{-3}$). The strict criterion thus admits genuine feature-specific intervention when it exists (Appendix A.6).

Failure mode A: random-dominant non-selective effect. Gemma L20 illustrates this pattern: cell means fall below $\mathrm{Sel}_{\mathrm{lp}} = 1$ for all four PII types (name 0.37, id 0.14, phone 0.27, email 0.09; Figure 1c). For Gemma L20/name, $|\Delta_{\mathrm{lp}}^{\mathrm{random}}| > |\Delta_{\mathrm{lp}}^{\mathrm{target}}|$ in 50/50 validation pairs and in 97.6% of 450 per-context observations; the same ordering holds on the discovery split ($\mathrm{Sel}_{\mathrm{lp}} = 0.25$). Since the random control is matched in strength, magnitude, and span-level coherence, the selected SAE direction is not the dominant feature-specific intervention point at this layer.

Failure mode B: feature selection collapse. In 3 of 9 (model, layer) cells (Gemma L20, Llama

L8, and Qwen L9) the discovery procedure selects the same top-1 feature for all four PII types, and none of these collapse cells passes the clean-strong criterion (Appendix A.7). In the representative case Llama L8, the selected feature has similar SAE activation magnitudes across PII types ($\leq 5\%$ variation: name 6.97, id 7.04, phone 6.77, email 7.01), yet its intervention effect is not type-agnostic: $|\Delta_{\text{lp}}^{\text{name}}| = 4.57$ is about 2.3 times larger than the average for id, phone, and email (≈ 1.96). This pattern admits two interpretations: (i) the feature is a generic PII-region marker whose ablation should affect all four PII types comparably, or (ii) the feature is not type-agnostic at the causal level. Interpretation (i) is inconsistent with the observed $2.3\times$ asymmetry under matched activation magnitudes, supporting (ii). The same asymmetry pattern holds in the other two collapse cells (Gemma L20: $6.8\times$, Qwen L9: up to $12\times$; Appendix A.9). Thus, shared feature selection does not imply a shared causal intervention effect.

5 A New Research Mission: Causally Grounded PII Suppression

The results of our selectivity experiments reveal a limitation not of SAE as a tool, but of the evaluation framework used to validate SAE-based PII suppression methods. The finding that feature-specific interventions are not statistically distinguishable from coherence-matched random interventions indicates that log-probability reduction, the primary success criterion in prior work, cannot confirm whether an intervention actually targets a PII-specific causal mechanism or merely introduces a generic perturbation. This concern is compounded by growing evidence that SAE feature directions may not be reliably distinguishable from random baselines in general settings (Korznikov et al., 2026; Ronge et al., 2026), suggesting that existing logprob-based evaluations cannot verify whether interventions target the causal pathways underlying PII leakage. From the perspective of Pearl's ladder of causation (Pearl, 2009; Pearl and Mackenzie, 2018), current practices remain at the level of association rather than intervention. We therefore propose two directions toward causally grounded PII suppression: identifying the causal pathways through which PII leakage occurs, and redesigning the evaluation framework to verify that interventions actually disrupt those pathways.

The first direction is to identify the causal pathways underlying PII leakage through circuit-level localization. Lasy et al. (2025) show that memorization initiation and maintenance in LLMs can be supported by distinct circuits. Applying circuit localization methods such as path patching (Wang et al., 2022) to PII leakage could identify which attention heads and MLP layers causally contribute to PII generation, providing a more principled basis for intervention than suppressing features merely correlated with PII.

The second direction is to adopt causal mediation analysis, introduced to NLP by Vig et al. (2020), as a framework for both identifying genuine causal mediators of PII leakage and verifying intervention effects. Applied to PII suppression, paired prompts with PII (x_1) and without PII (x_0) are constructed, and SAE feature f activations are patched across conditions to measure the Natural Indirect Effect (NIE), the extent to which f mediates PII generation. Features with significant NIEs serve as principled intervention targets, and the same framework verifies that a given intervention actually disrupts the identified causal mechanism rather than merely perturbing model activations.

This shift—from correlation-based feature discovery to causally grounded circuit identification, and from log-probability-based measurement to causal verification through mediation analysis—defines the path forward.

6 Conclusion

Across 36 (model, layer, PII type) configurations, this work empirically shows that logprob reduction, the standard evaluation signal in SAE-based PII suppression studies, does not distinguish feature-specific intervention from generic magnitude perturbation. Only one cell (Llama L16/name) passes both the coherence-matched random control and the rank-aware metric. This confirms that our evaluation protocol can identify genuine feature-specific effects when they exist, while showing that, in the remaining 35 cells, conventional evaluation cannot verify whether the selected feature is causally involved in PII leakage. Multi-metric evaluation is a diagnostic tool, not a final solution; the fundamental goal is to identify the causal pathways underlying PII leakage. We propose causally grounded PII suppression—through circuit-level localization and causal mediation analysis—as a new research mission for NLP.

Limitations

This study has several limitations.

Model scale and domain. Our experiments are limited to 8B/9B-class general-purpose LLMs. We do not test whether the same patterns hold for substantially larger models, closed-source models, or domain-specialized LLMs, mainly because task-specific SAE analysis requires collecting large-scale activations and training separate SAEs for each model and layer. In particular, domain-specialized models may exhibit different activation distributions due to their pretraining and fine-tuning corpora; developing SAE training protocols suitable for such models, and testing whether our findings replicate on them, remain future work.

Hidden-space vs. z-space intervention. Our intervention preserves the SAE reconstruction-error term $(\mathbf{h}_t - \hat{\mathbf{h}}_t)$ that a full encode-decode pipeline (as in PrivacyScalpel) would discard. While the selectivity ratio is invariant to this error term, the absolute magnitudes of Δ_{lp} and Δ_{br} may shift under z-space intervention. Direct z-space replication is left to future work.

SAE capacity. We evaluate task-specific SAEs with expansion factor $\times 8$ and fixed sparsity $k = 32$. We do not ablate larger expansion factors such as $\times 16$ or $\times 32$, alternative sparsity levels, or different SAE objectives. Since SAE capacity may affect feature isolation, future work should test whether the failure modes identified here, especially feature selection collapse (Failure mode B) and random-dominant non-selective effects (Failure mode A), persist under larger or differently trained SAEs.

Synthetic data. Our evaluation uses a synthetic medical PII corpus. We avoid real patient records due to ethical and regulatory constraints. Synthetic data allows us to control PII values, clinical context, and entity-level disjoint splits, but it cannot fully capture the linguistic diversity, formatting noise, or annotation ambiguity of real medical records. Whether the same patterns hold in real-world private corpora remains open. At the same time, our core claim is methodological rather than dataset-specific: logprob-only evaluation can fail to distinguish feature-specific interventions from generic magnitude perturbations.

Selective layer coverage. We train and evaluate SAEs at three pre-specified depth-proportional layers, approximately 25%, 50%, and 75% of each model's depth. This design avoids choosing layers based on downstream intervention outcomes, but it is not an exhaustive layer-wise search. Other layers may contain stronger feature-specific intervention directions, or may exhibit different failure modes. Exhaustive layer-wise SAE analysis is left for future work.

Single-feature intervention. Our experiments focus on single-feature hidden-space interventions using one selected SAE feature. Thus, when a selected feature is indistinguishable from random controls or produces anti-suppression, this does not rule out multi-feature or circuit-level interventions. Rather, our results suggest that PII leakage may arise through causal pathways more complex than a single SAE feature; identifying and intervening on such pathways remains a key direction for future work.

Extraction risk and utility. We do not systematically evaluate full adversarial extraction attacks or downstream utility benchmarks. Our metrics (gold PII span logprob, a rank-aware extraction-cost proxy, and coherence-matched random-control selectivity) are diagnostic signals, not privacy guarantees against arbitrary attackers. We also do not measure the effect of interventions on external tasks such as medical QA, general language ability, or instruction following. Future work should combine our diagnostic evaluation with actual extraction attacks and utility benchmarks.

Ethical considerations

This work studies SAE-based PII suppression in LLMs, motivated by privacy concerns surrounding LLM memorization of sensitive information. To avoid exposing real patient data, all PII used in this study is fully synthetic. The synthetic medical PII corpus and clinical notes were generated specifically for the controlled study of intervention behavior and do not contain any real-world identifying information. Our results highlight that prior SAE-based PII suppression evaluations may overestimate genuine privacy protection. While this finding could inform improved privacy defenses, we note that the diagnostic methodology operates at the level of evaluation and does not enable new attack capabilities beyond what is already accessible to any black-box adversary. We encourage future work to combine the multi-metric diagnostic framework with extraction-attack benchmarks to

verify substantive privacy guarantees.

References

Trenton Bricken, Adly Templeton, Joshua Batson, Brian Chen, Adam Jermyn, Tom Conerly, Nicholas L. Turner, Cem Anil, Carson Denison, Amanda Askell, Robert Lasenby, Yifan Wu, Shauna Kravec, Nicholas Schiefer, Tim Maxwell, Nicholas Joseph, Alex Tamkin, Karina Nguyen, Brayden McLean, and 5 others. 2023. Towards monosemanticity: Decomposing language models with dictionary learning. *Transformer Circuits Thread*.

Nicholas Carlini, Daphne Ippolito, Matthew Jagielski, Katherine Lee, Florian Tramèr, and Chiyuan Zhang. 2023. Quantifying memorization across neural language models. In *The Eleventh International Conference on Learning Representations*.

Nicholas Carlini, Florian Tramèr, Eric Wallace, Matthew Jagielski, Ariel Herbert-Voss, Katherine Lee, Adam Roberts, Tom Brown, Dawn Song, Úlfar Erlingsson, Alina Oprea, and Colin Raffel. 2021. Extracting training data from large language models. In *30th USENIX Security Symposium (USENIX Security 21)*, pages 2633–2650. USENIX Association.

Ruizhe Chen, Tianxiang Hu, Yang Feng, and Zuozhu Liu. 2024a. Learnable privacy neurons localization in language models. In *Proceedings of the 62nd Annual Meeting of the Association for Computational Linguistics (Volume 2: Short Papers)*, pages 256–264, Bangkok, Thailand. Association for Computational Linguistics.

Zhiyu Zoey Chen, Jing Ma, Xinlu Zhang, Nan Hao, An Yan, Armineh Nourbakhsh, Xianjun Yang, Julian McAuley, Linda Petzold, and William Yang Wang. 2024b. A survey on large language models for critical societal domains: Finance, healthcare, and law. *Computing Research Repository*, arXiv:2405.01769.

Hoagy Cunningham, Aidan Ewart, Logan Riggs, Robert Huben, and Lee Sharkey. 2023. Sparse autoencoders find highly interpretable features in language models. *Computing Research Repository*, arXiv:2309.08600.

Ahmed Frikha, Muhammad Reza Ar Razi, Krishna Kanth Nakka, Ricardo Mendes, Xue Jiang, and Xuebing Zhou. 2025. PrivacyScalpel: Enhancing LLM privacy via interpretable feature intervention with sparse autoencoders. In *Proceedings of the 8th BlackboxNLP Workshop: Analyzing and Interpreting Neural Networks for NLP*, pages 226–238, Suzhou, China. Association for Computational Linguistics.

Leo Gao, Tom Dupré la Tour, Henk Tillman, Gabriel Goh, Rajan Troll, Alec Radford, Ilya Sutskever, Jan Leike, and Jeffrey Wu. 2025. Scaling and evaluating sparse autoencoders. In *The Thirteenth International Conference on Learning Representations*, pages 26721–26754.

Gemma Team. 2024. Gemma 2: Improving open language models at a practical size. *arXiv preprint arXiv:2408.00118*.

Aaron Grattafiori, Abhimanyu Dubey, Abhinav Jauhri, Abhinav Pandey, Abhishek Kadian, Ahmad Al-Dahle, Aiesha Letman, Akhil Mathur, Alan Schelten, Alex Vaughan, and 1 others. 2024. The Llama 3 herd of models. *arXiv preprint arXiv:2407.21783*.

Edward J. Hu, Yelong Shen, Phillip Wallis, Zeyuan Allen-Zhu, Yuanzhi Li, Shean Wang, Lu Wang, and Weizhu Chen. 2022. LoRA: Low-rank adaptation of large language models. In *The Tenth International Conference on Learning Representations*.

Daphne Ippolito, Florian Tramèr, Milad Nasr, Chiyuan Zhang, Matthew Jagielski, Katherine Lee, Christopher A. Choquette-Choo, and Nicholas Carlini. 2022. Preventing verbatim memorization in language models gives a false sense of privacy. *Computing Research Repository*, arXiv:2210.17546.

Ganesh Jawahar, Benoît Sagot, and Djamé Seddah. 2019. What does BERT learn about the structure of language? In *Proceedings of the 57th Annual Meeting of the Association for Computational Linguistics*, pages 3651–3657, Florence, Italy. Association for Computational Linguistics.

Mingyu Jin, Qinkai Yu, Jingyuan Huang, Qingcheng Zeng, Zhenting Wang, Wenyue Hua, Haiyan Zhao, Kai Mei, Yanda Meng, Kaize Ding, Fan Yang, Mengnan Du, and Yongfeng Zhang. 2025. Exploring concept depth: How large language models acquire knowledge and concept at different layers? In *Proceedings of the 31st International Conference on Computational Linguistics*, pages 558–573, Abu Dhabi, UAE. Association for Computational Linguistics.

Siwon Kim, Sangdoo Yun, Hwaran Lee, Martin Gubri, Sungroh Yoon, and Seong Joon Oh. 2023. ProPILE: Probing privacy leakage in large language models. In *Advances in Neural Information Processing Systems 36 (NeurIPS 2023)*.

Anton Korznikov, Andrey Galichin, Alexey Dontsov, Oleg Rogov, Ivan Oseledets, and Elena Tutubalina. 2026. Sanity checks for sparse autoencoders: Do SAEs beat random baselines? *Computing Research Repository*, arXiv:2602.14111.

Ilya Lasy, Peter Knees, and Stefan Woltran. 2025. Understanding verbatim memorization in LLMs through circuit discovery. In *Proceedings of the First Workshop on Large Language Model Memorization (L2M2)*, pages 83–94, Vienna, Austria. Association for Computational Linguistics.

Eric Lehman, Sarthak Jain, Karl Pichotta, Yoav Goldberg, and Byron C. Wallace. 2021. Does BERT pretrained on clinical notes reveal sensitive data? In *Proceedings of the 2021 Conference of the North American Chapter of the Association for Computational Linguistics: Human Language Technologies*,

pages 946–959, Online. Association for Computational Linguistics.

Krishna Kanth Nakka, Ahmed Frikha, Ricardo Mendes, Xue Jiang, and Xuebing Zhou. 2024. PII-Scope: A benchmark for training data PII leakage assessment in LLMs. *Computing Research Repository*, arXiv:2410.06704.

Judea Pearl. 2009. *Causality: Models, Reasoning, and Inference*, 2nd edition. Cambridge University Press, Cambridge, UK.

Judea Pearl and Dana Mackenzie. 2018. *The Book of Why: The New Science of Cause and Effect*. Basic Books, New York, NY.

Raphael Ronge, Markus Maier, and Frederick Eberhardt. 2026. When the coffee feature activates on coffins: An analysis of feature extraction and steering for mechanistic interpretability. *Computing Research Repository*, arXiv:2601.03047.

Ian Tenney, Dipanjan Das, and Ellie Pavlick. 2019. BERT rediscovers the classical NLP pipeline. In *Proceedings of the 57th Annual Meeting of the Association for Computational Linguistics*, pages 4593–4601, Florence, Italy. Association for Computational Linguistics.

Jesse Vig, Sebastian Gehrmann, Yonatan Belinkov, Sharon Qian, Daniel Nevo, Yaron Singer, and Stuart Shieber. 2020. Investigating gender bias in language models using causal mediation analysis. In *Advances in Neural Information Processing Systems*, volume 33, pages 12388–12401.

Kevin Wang, Alexandre Variengien, Arthur Conmy, Buck Shlegeris, and Jacob Steinhardt. 2022. Interpretability in the wild: a circuit for indirect object identification in GPT-2 small. *Computing Research Repository*, arXiv:2211.00593.

An Yang, Anfeng Li, Baosong Yang, Beichen Zhang, Binyuan Hui, Bo Zheng, Bowen Yu, Chang Gao, Chengen Huang, Chenxu Lv, and 1 others. 2025. Qwen3 technical report. *Computing Research Repository*, arXiv:2505.09388.

A Appendix

A.1 Additional Background on PII Suppression

A.1.1 PII Memorization in LLMs

LLMs can memorize PII contained in their pretraining data, which may then be leaked through verbatim reproduction when the model is prompted with a particular prefix. Carlini et al. (2021) demonstrated that verbatim sequences containing PII, including names, phone numbers, and email addresses, can be extracted from GPT-2 using only black-box queries, and showed that memorization becomes more severe as model size increases (Carlini et al., 2023). Ippolito et al. (2022) further showed that even a Bloom-filter-based defense that perfectly prevents verbatim memorization can be bypassed by minimally modified style-transfer prompts, allowing memorized information to still be leaked. These findings warn that defenses satisfying surface-level metrics do not necessarily guarantee substantive privacy protection, closely aligning with the limitations of evaluation protocols discussed in the main section.

A.1.2 SAE-based PII Suppression

With advances in interpretability research on the internal representations of LLMs, studies on PII suppression has increasingly shifted toward interventions on model internals. Chen et al. (2024a) combined learnable binary weight masks with adversarial training to localize and deactivate privacy neurons associated with PII memorization, aiming to suppress PII leakage. However, such neuron-level approaches are limited in both interpretability and precision due to polysemanticity, as individual neurons may represent multiple concepts simultaneously. Therefore, SAE-based approaches have been proposed as a more interpretable alternative. By decomposing LLM activations into high-dimensional sparse feature spaces, SAEs aim to learn monosemantic representations in which individual features correspond to specific concepts (Bricken et al., 2023; Cunningham et al., 2023). PrivacyScalpel (Frikha et al., 2025) is a representative study that applies SAEs to PII suppression. It first identifies the layer where PII representations are most concentrated through feature probing, trains a k-SAE on the activations of that layer to isolate privacy-sensitive features in a monosemantic space, and then suppresses PII-related features through feature ablation and vector steering. On Gemma2-2B and Llama2-7B, PrivacyScalpel reportedly reduces the email leakage rate from 5.15% to 0.0% while preserving more than 99.4% of the original model performance, demonstrating a stronger privacy-utility trade-off compared with neuron-level interventions. However, its evaluation does not determine whether the reduction in email leakage results from selective suppression of PII-sensitive features or from a generic activation perturbation that degrades the model's ability to generate email-formatted strings.

A.1.3 Critiques of SAE Feature Reliability

Alongside the rapid adoption of SAE-based interpretability research, recent work has increasingly raised critical questions about the substantive meaning and reliability of SAE features. Ronge et al. (2026) stress-test Anthropic-style SAE-based feature steering using Llama 3.1 and find that steering effects exhibit substantial fragility depending on layer selection, steering magnitude, and context. These findings suggest that SAE feature directions may function only under limited conditions, casting doubt on whether they provide stable and generalizable causal effects. Furthermore, Korznikov et al. (2026) systematize this concern by showing that random-feature baselines can perform comparably to fully trained SAEs across interpretability, sparse probing, and causal editing evaluations, raising a fundamental question about whether SAE features provide meaningful information. Our paper extends this critique to the privacy domain by examining it in the concrete setting of PII suppression. Specifically, we use coherence-matched random controls to directly test whether evaluation metrics used in prior PII suppression studies, such as email leakage rate, can distinguish feature-specific interventions from generic activation perturbations. In doing so, we instantiate Korznikov et al. (2026)'s general critique as a methodological critique of evaluation practices in SAE-based PII suppression.

A.2 Models, Data, and SAE Training

All experiments, including SAE training and intervention evaluation, were conducted on a single NVIDIA RTX 4090 (24 GB VRAM).

Models and data. We use three LoRA fine-tuned LLMs: two 8B-class models (Llama-3.1-8B-Instruct and Qwen3-8B) and one 9B-class model (Gemma-2-9B), all fine-tuned on the same synthetic medical PII corpus. These publicly available models are used under their respective licenses: Llama-3.1-8B-Instruct under the Llama 3.1 Community License (Meta Platforms, Inc.), Qwen3-8B under the Apache 2.0 License (Alibaba Cloud), Gemma-2-9B under the Gemma Terms of Use (Google). Each example appends four PII fields (name, patient ID, phone number, and email) to the end of a clinical note. Table 1 summarizes the hidden dimension, total number of layers, and the task-specific SAE training layers for each model.

For evaluation, we use a total of 600 PII pairs, with feature discovery and final evaluation performed on disjoint splits (Table 2). Task-specific SAEs are trained on a separate 50k synthetic clinical note corpus with no entity-level overlap with either the LLM fine-tuning corpus or the evaluation pairs. This disjoint design ensures that the SAEs learn general contextual representations associated with PII, rather than memorizing specific PII entities from the evaluation set or those seen during LLM fine-tuning.

Model	Depth	d_{model}	SAE layers
Gemma-2-9B	42	3584	9, 20, 31
Llama-3.1-8B-Instruct	32	4096	8, 16, 24
Qwen3-8B	36	4096	9, 18, 27

Table 1: Model and layer configuration. SAE layers are selected at approximately 25%, 50%, 75% depth.

Split	Pair indices	Purpose
Discovery	0–9	Feature discovery
Diagnostic	0–19	Reconstruction diagnostics
Validation	300–349	Main multi-metric evaluation
SAE training	separate 50k corpus	Task-SAE training

Table 2: Data split used for feature discovery, diagnostics, and final evaluation. The SAE training corpus is entity-level disjoint from the 600 evaluation pairs.

SAE training. For each model, we train top-k sparse autoencoders at three depth-proportional layers, corresponding to approximately 25%, 50%, and 75% of the model depth. This design follows prior work that compares transformer representations at fixed relative depths (Jin et al., 2025), as well as studies showing that linguistic and task-relevant information varies across layers (Tenney et al., 2019; Jawahar et al., 2019). The sampled layers are not chosen based on SAE quality metrics or downstream intervention performance; thus, any layer-dependent differences observed in our experiments should be interpreted as differences across model depth rather than as outcome-driven selection bias. All SAEs are trained with the same hyperparameters (Table 3).

Hyperparameter	Value
Expansion factor	$\times 8$
Sparsity k	32
Auxiliary loss weight	0.25
Dead feature threshold	1000 inactive steps
Training steps	80,000
Batch size	4,096 tokens
Learning rate	3×10^{-4}

Table 3: Task-specific SAE training hyperparameters.

All trained SAEs achieve over 98.8% variance explained on the held-out SAE training sub-

set. However, corpus-level reconstruction quality does not necessarily reflect quality at intervention-relevant PII token positions, so we separately report PII-position reconstruction error in Table 4.

Model	Layer	Rel. err. all	Rel. err. PII	Cosine PII
Gemma-2-9B	9	5.11%	2.78%	0.9996
Gemma-2-9B	20	10.28%	6.38%	0.9980
Gemma-2-9B	31	9.74%	8.82%	0.9961
Llama-3.1-8B-Instruct	8	5.20%	1.99%	0.9998
Llama-3.1-8B-Instruct	16	6.77%	13.53%	0.9907
Llama-3.1-8B-Instruct	24	10.45%	39.20%	0.9192
Qwen3-8B	9	5.88%	2.11%	0.9998
Qwen3-8B	18	8.60%	2.62%	0.9997
Qwen3-8B	27	11.28%	35.59%	0.9337

Table 4: SAE reconstruction quality across nine (model, layer) cells. Relative error is $\|\mathbf{h} - \hat{\mathbf{h}}\|/\|\mathbf{h}\|$; "all" averages over all token positions, "PII" over PII token positions only. Cosine similarity is computed at PII token positions. Deep layers (Llama L24, Qwen L27) show higher PII-position reconstruction error.

A.3 Prompt Templates

To evaluate cross-template robustness, we use nine prompt templates. T0 follows the original training format, while T1–T8 introduce variations including different label lengths, natural language phrasing, Korean labels, JSON format, and narrative format (Table 5).

ID	Example format for name PII	Context
T0	`Patient Name: {name}`	all 4 PII fields
T1	`Patient Name: {name}`	target PII only
T2	`Name: {name}`	target PII only
T3	`Full name: {name}`	target PII only
T4	`The patient's name is {name}`	target PII only
T5	`환자 이름: {name}`	target PII only
T6	`Patient: {name}`	target PII only
T7	`{"name": "{name}"}`	target PII only
T8	`The patient, {name}, ...`	target PII only

Table 5: Prompt templates used for cross-template evaluation. T0 retains the original training prompt that contains all four PII fields (name, patient ID, phone, email) together; T1–T8 isolate the target PII field only, with varying label formats. T8 is abbreviated (full text: "The patient, {name}, presented with chest pain."). The same template family is adapted to patient ID, phone number, and email PII.

A.4 Feature Discovery, Intervention, and Metrics

Feature discovery. Feature discovery is performed only on the discovery split. We first extract hidden states near the PII marker and encode them with the SAE to obtain sparse activations z. For each PII type, we select non-dead features with large mean activation magnitude as candidates, where a dead feature is one that has not been activated for a fixed inactivity window by the end of SAE training. For each candidate, we apply hidden-space intervention directly and designate as the selected feature for each (model, layer, PII type) the one that yields the largest reduction in gold PII span logprob on the discovery split. The selected feature is fixed before validation, and final results are reported only on the held-out validation split.

Hidden-space intervention. Our main intervention operates in hidden space rather than in SAE latent space. Instead of modifying the SAE latent and reconstructing the hidden state through the decoder, we directly steer the original LLM hidden state using the decoder direction of the selected SAE feature. At token position t in layer ℓ:

$$h'_t = h_t + \alpha \cdot z_t[f] \cdot W_{\text{dec}}[f],$$

where $z_t[f]$ is the SAE activation of selected feature f at token t, and $W_{\text{dec}}[f]$ is its decoder direction. We fix $\alpha = -2$ for all main experiments and do not retune it per model, layer, or PII type. The intervention hook is applied to all token positions in the forward pass; however, because top-k SAE activations are sparse, the intervention term vanishes automatically at tokens where the selected feature is inactive ($z_t[f] = 0$). Thus, we do not use an explicit PII-span intervention mask, and evaluation is restricted to the gold PII span.

Coherence-matched random direction control. To distinguish feature-specific effects from generic magnitude perturbations, we compare each selected feature intervention against a coherence-matched random direction control. The random control preserves the same α and token-wise intervention magnitude, but replaces the SAE decoder direction with an isotropic random unit vector. For the target contribution $c_t = z_t[f]W_{\text{dec}}[f]$, we compute $m_t = \|c_t\|_2$. In each forward pass, we sample one isotropic random unit vector r and share it across all intervened token positions, matching the span-level direction coherence of the selected-feature intervention, which uses the same $W_{\text{dec}}[f]$ at all positions:

$$h'_t = h_t + \alpha \cdot m_t \cdot r.$$

Thus, the selected-feature intervention and the random control share the same intervention strength, token-wise magnitude pattern, and span-level direction coherence; their intended difference is only

whether the direction is the selected SAE decoder direction or an isotropic random direction. We average random-control results over three independent seeds.

Metrics and selectivity. We evaluate each intervention using two signed metrics. The first is the change in mean log-probability of the gold PII span,

$$\Delta_{\mathrm{lp}} = \mathrm{lp}_{\mathrm{int}} - \mathrm{lp}_{\mathrm{base}},$$

where $\Delta_{\mathrm{lp}} < 0$ indicates reduced gold PII likelihood after intervention. The second is the change in a rank-aware extraction-cost proxy,

$$b_{\mathrm{rank}}(y) = \sum_{t \in y} \log_2(\mathrm{rank}_t),$$

with intervention-induced change $\Delta_{\mathrm{br}} = b_{\mathrm{rank,int}} - b_{\mathrm{rank,base}}$; $\Delta_{\mathrm{br}} > 0$ indicates that gold PII tokens move backward in the candidate ranking, increasing the rank-based extraction cost. Selectivity is defined as the effect magnitude of the selected-feature intervention (denoted with the ^{target} superscript) divided by the effect magnitude of the random direction control:

$$\mathrm{Sel}_{\mathrm{lp}} = \frac{|\Delta_{\mathrm{lp}}^{\mathrm{target}}|}{|\Delta_{\mathrm{lp}}^{\mathrm{random}}|}, \quad \mathrm{Sel}_{\mathrm{br}} = \frac{|\Delta_{\mathrm{br}}^{\mathrm{target}}|}{|\Delta_{\mathrm{br}}^{\mathrm{random}}|}.$$

Selectivity is a magnitude-based diagnostic for feature-specificity; the directionality of suppression or anti-suppression is interpreted separately through the signs of raw Δ_{lp} and Δ_{br}.

Category thresholds. We use threshold-based categories to summarize intervention behavior in figures and summary tables. These categories are not used for intervention tuning; they serve only as post-hoc labels for interpreting the results. Each cell is assigned to one of seven categories based on five criteria, summarized in Tables 6 and 7.

Criterion	Meaning
$\Delta_{\mathrm{lp}} \leq -0.3$	logprob suppression
$\Delta_{\mathrm{br}} \geq +1.0$	rank-cost improvement
$\Delta_{\mathrm{lp}} > +0.1$	logprob anti-suppression
$\Delta_{\mathrm{br}} < -0.3$	rank-cost degradation
$\mathrm{Sel}_{\mathrm{lp}}, \mathrm{Sel}_{\mathrm{br}} \geq 5$	strong feature-specificity

Table 6: Five criteria used for category labels.

Category	Definition
clean-strong	$\Delta_{\mathrm{lp}} \leq -0.3$, $\Delta_{\mathrm{br}} \geq +1.0$, $\mathrm{Sel}_{\mathrm{lp}}, \mathrm{Sel}_{\mathrm{br}} \geq 5$
clean-weak	$\Delta_{\mathrm{lp}} \leq -0.3$, $\Delta_{\mathrm{br}} \geq +1.0$, Sel < 5 on $\geq$1 metric
anti	$\Delta_{\mathrm{lp}} > +0.1$ or $\Delta_{\mathrm{br}} < -0.3$
lp-only	$\Delta_{\mathrm{lp}} \leq -0.3$ but $\Delta_{\mathrm{br}} < +1.0$
br-only	$\Delta_{\mathrm{br}} \geq +1.0$ but $\Delta_{\mathrm{lp}} > -0.3$
inactive	$z_t[f] \approx 0$
noise	none of the above

Table 7: Category definitions used for post-hoc labeling. Each cell is assigned exactly one category. Raw Δ and Sel values are reported alongside category labels.

A.5 Full Per-Cell Results

The categorical analysis in Section 4 is computed from cell-level means over all 36 cells. Table 8 reports, for every cell, the Δ_{lp}, Δ_{br}, both selectivity values, and the category label for the selected-feature intervention and its coherence-matched random control. All values are averaged over 50 validation pairs $\times$ 9 prompt templates $=$ 450 evaluation contexts.

A.6 Per-Template Breakdown

This provides the supporting data for the cross-template claims in Section 4, including the 9-template consistency of Failure mode A and the OOD-template robustness of Llama L16/name. Due to space constraints, Table 9 reports full per-template values only for cells directly discussed in the main text.

A.7 Selected Feature Inventory

Table 10 reports the feature ID selected by the discovery procedure for each (model, layer, PII type). We group the 9 (model, layer) cells by feature-sharing pattern. All full feature-selection collapse cells (Gemma L20, Llama L8, and Qwen L9) fail to pass the clean-strong criterion. The only clean-strong configuration, Llama L16/name, occurs in a non-full-collapse cell. Thus, repeated selection of the same feature across multiple PII types does not guarantee clean-strong feature-specific suppression.

As an additional diagnostic, we measure the SAE activation $z_t[f]$ of Llama L8 feature 16363, the clearest full-collapse case, across the four PII types. Its activation magnitude varies by at most 5% across types (name 6.97, id 7.04, phone 6.77, email 7.01; averaged over 50 validation pairs). Thus, the selected feature appears similar across PII types at both the selection and activation levels, but its intervention effect remains type-biased, as reported under Failure mode B in Section 4.

A.8 Failure Mode A Diagnostic: Gemma L20

Gemma L20 exhibits Failure mode A, the random-dominant non-selective pattern. For Gemma

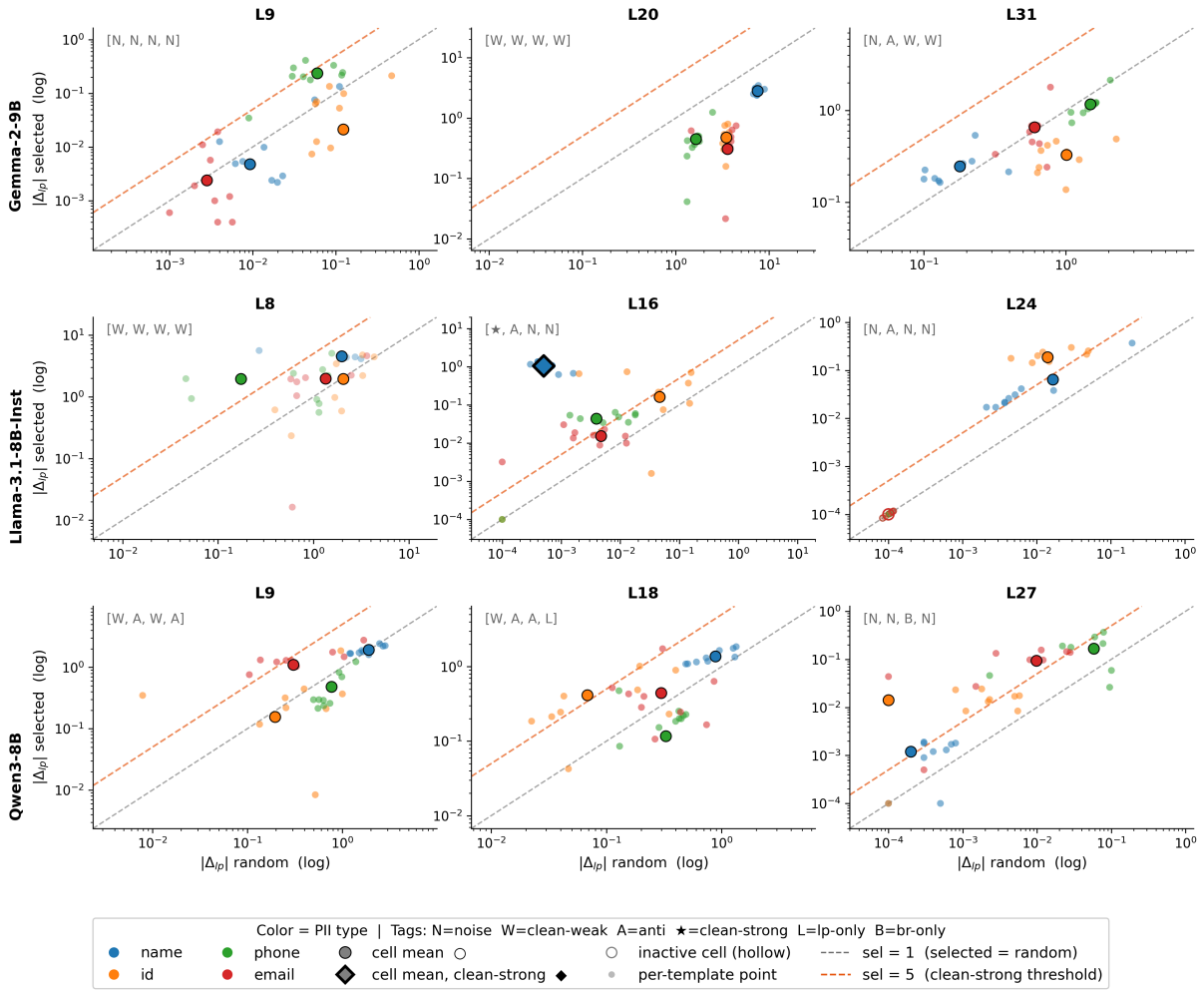

Figure 2: Selected feature intervention effect ($|\Delta_{\mathrm{lp}}^{\mathrm{target}}|$, y-axis) versus coherence-matched random direction effect ($|\Delta_{\mathrm{lp}}^{\mathrm{random}}|$, x-axis), per (model, layer, PII type) configuration; both axes log scale. Large markers indicate cell mean over 9 templates $\times$ 50 validation pairs (450 evaluation contexts); small dots indicate per-template means within a cell. Gray dashed: $\mathrm{Sel}_{\mathrm{lp}} = 1$ (target = random). Orange dashed line: $\mathrm{Sel}_{\mathrm{lp}} = 5$ (clean-strong selectivity threshold). Diamond (♦): cell satisfying all clean-strong criteria; hollow markers: inactive configurations ($z_t[f] \approx 0$). Of 36 configurations, only Llama L16/name qualifies as clean-strong. Top-left tag in each subplot encodes category labels for [name, id, phone, email] (N=noise, W=clean-weak, A=anti, L=lp-only, B=br-only, ★=clean-strong). The clean-strong label (♦) reflects the full multi-metric criterion including rank-aware Δ_{br} and signed-metric checks.

L20/name, the coherence-matched random direction produces a larger absolute logprob effect than the selected SAE direction in all 50 validation pairs: $|\Delta_{\mathrm{lp}}^{\mathrm{random}}| > |\Delta_{\mathrm{lp}}^{\mathrm{target}}|$ holds in 50/50 pairs. At the per-(pair, template) context level, the same inequality holds in 439/450 contexts (97.6%). The pattern is observed on both the discovery split ($\mathrm{Sel}_{\mathrm{lp}} = 0.25$) and the validation split ($\mathrm{Sel}_{\mathrm{lp}} = 0.37$). Because the random control matches the selected-feature intervention in intervention strength, token-wise magnitude, and span-level direction coherence, this random-dominant pattern cannot be attributed to a larger random-vector norm. Rather, it indicates that the selected SAE direction is not more selective than a magnitude-matched random direction in this layer. We do not determine whether this arises from the selected feature's failure to generalize, from the dominant PII-related direction not being captured by a single SAE feature, or from the selected direction being weakly misaligned with the intervention-relevant direction.

A.9 Failure Mode B Diagnostic: Collapse Cell Asymmetry

The three full-collapse cells (Gemma L20, Llama L8, Qwen L9) discussed in Section 4 all exhibit type-asymmetric intervention effects despite shared feature selection and matched SAE activation mag-

Model	Layer/PII	$\Delta^{\mathrm{T}}_{\mathrm{lp}}$	$\Delta^{\mathrm{R}}_{\mathrm{lp}}$	$\mathrm{Sel}_{\mathrm{lp}}$	$\Delta^{\mathrm{T}}_{\mathrm{br}}$	$\Delta^{\mathrm{R}}_{\mathrm{br}}$	$\mathrm{Sel}_{\mathrm{br}}$	Category
Gemma	9/name	-0.005	$+0.009$	0.52	$+0.053$	-0.079	0.68	noise
Gemma	9/id	$+0.021$	-0.123	0.17	$+0.111$	$+0.310$	0.36	noise
Gemma	9/phone	-0.235	-0.060	3.95	$+0.144$	-0.040	3.56	noise
Gemma	9/email	$+0.002$	$+0.003$	0.88	$+0.007$	$+0.004$	1.54	noise
Gemma	20/name	-2.805	-7.524	0.37	$+4.806$	$+12.906$	0.37	clean-weak
Gemma	20/id	-0.475	-3.460	0.14	$+3.166$	$+18.171$	0.17	clean-weak
Gemma	20/phone	-0.450	-1.646	0.27	$+6.800$	$+19.997$	0.34	clean-weak
Gemma	20/email	-0.308	-3.583	0.09	$+5.806$	$+33.087$	0.17	clean-weak
Gemma	31/name	-0.246	-0.179	1.38	-0.085	$+0.269$	0.32	noise
Gemma	31/id	-0.329	-1.006	0.33	-0.557	$+4.963$	0.11	anti
Gemma	31/phone	-1.168	-1.486	0.79	$+6.891$	$+7.833$	0.88	clean-weak
Gemma	31/email	-0.655	-0.602	1.09	$+3.034$	$+3.279$	0.93	clean-weak
Llama	8/name	-4.565	-1.967	2.32	$+6.141$	$+2.818$	2.18	clean-weak
Llama	8/id	-1.958	-2.047	0.96	$+7.988$	$+7.947$	1.00	clean-weak
Llama	8/phone	-1.951	-0.174	11.21	$+14.422$	$+4.221$	3.42	clean-weak
Llama	8/email	-1.969	-1.332	1.48	$+20.642$	$+17.072$	1.21	clean-weak
Llama	16/name	-1.060	-0.001	1995	$+1.465$	$+0.010$	147	**clean-strong**
Llama	16/id	$+0.162$	-0.046	3.51	-0.338	$+0.164$	2.06	anti
Llama	16/phone	$+0.043$	$+0.004$	11.02	-0.071	$+0.007$	10.04	noise
Llama	16/email	-0.015	$+0.005$	3.24	$+0.064$	-0.005	12.96	noise
Llama	24/name	-0.065	$+0.017$	3.94	$+0.127$	$+0.032$	3.98	noise
Llama	24/id	$+0.189$	$+0.014$	13.42	-0.291	-0.015	19.70	anti
Llama	24/phone	$+0.000$	-0.000	—	$+0.000$	$+0.000$	—	inactive
Llama	24/email	$+0.000$	$+0.000$	—	$+0.000$	$+0.000$	—	inactive
Qwen	9/name	-1.916	-1.896	1.01	$+2.530$	$+2.380$	1.06	clean-weak
Qwen	9/id	$+0.155$	-0.196	0.79	$+3.324$	$+3.425$	0.97	anti
Qwen	9/phone	-0.483	-0.770	0.63	$+11.316$	$+6.979$	1.62	clean-weak
Qwen	9/email	$+1.106$	$+0.305$	3.62	$+5.797$	$+4.995$	1.16	anti
Qwen	18/name	-1.381	-0.883	1.56	$+1.972$	$+1.019$	1.94	clean-weak
Qwen	18/id	-0.413	-0.068	6.04	-0.442	$+0.719$	0.61	anti
Qwen	18/phone	$+0.117$	$+0.327$	0.36	$+0.557$	$+0.328$	1.70	anti
Qwen	18/email	-0.442	$+0.297$	1.49	$+0.711$	$+1.076$	0.66	lp-only
Qwen	27/name	-0.001	-0.000	5.49	$+0.009$	$+0.000$	—	noise
Qwen	27/id	-0.014	$+0.000$	115.1	$+0.018$	-0.005	3.80	noise
Qwen	27/phone	-0.169	$+0.058$	2.92	$+1.091$	-0.013	86.38	br-only
Qwen	27/email	-0.093	-0.010	9.51	$+0.344$	$+0.064$	5.41	noise

Table 8: Full per-cell results over 36 configurations. T = target (selected feature); R = coherence-matched random. All values are means over 50 validation pairs $\times$ 9 templates. Inactive configurations have $z_t[f] \approx 0$ across all templates, so neither effect nor selectivity is well-defined.

nitudes ($\leq 5\%$ variation across PII types in each cell). Table 11 summarizes the per-type $\Delta_{lp}^{\text{target}}$ values.

A.10 Threshold Sensitivity

The "47% $\rightarrow$ 3%" reduction reported in Section 4 is computed using our default conjunctive criterion: $\Delta_{\mathrm{lp}} \leq -0.3$, $\Delta_{\mathrm{br}} \geq +1.0$, $\mathrm{Sel}_{\mathrm{lp}} \geq 5$, $\mathrm{Sel}_{\mathrm{br}} \geq 5$, and no anti-suppression. To test whether this conclusion depends on particular cutoffs, we perform sensitivity analyses along three axes: single-metric selectivity, dual-metric selectivity, and magnitude gate.

Selectivity threshold (single vs dual). Table 12 reports the number of passing cells as the selectivity threshold is varied, comparing single-metric ($\mathrm{Sel}_{\mathrm{lp}}$ only) and dual-metric ($\mathrm{Sel}_{\mathrm{lp}}$ AND $\mathrm{Sel}_{\mathrm{br}}$) criteria. At ≥ 5, single-metric admits 2 cells while dual-metric admits 1 (Llama L16/name); the additional cell filtered by dual-metric is Llama L8/phone ($\mathrm{Sel}_{\mathrm{br}} = 3.4$), confirming the necessity of including $\mathrm{Sel}_{\mathrm{br}}$. Even the loosest single-metric threshold (≥ 2) admits only 3/36 (8.3%), far below the 17/36 (47%) under logprob-only evaluation.

Magnitude gate. Table 13 reports the number of passing cells when we vary the magnitude gate while keeping the selectivity threshold fixed at ≥ 5.

Across all three sensitivity axes, even the loosest setting admits at most 3/36 clean-strong cells (8.3%). Thus, the central conclusion of this work is robust to threshold choice: the 47% apparent success rate under logprob-only evaluation collapses to a single clean-strong cell under strict multi-metric evaluation.

A.11 α Sensitivity

We fix $\alpha = -2$ in all main experiments. To verify that our diagnostic conclusions are

Template	$\Delta^{\mathrm{T}}_{\mathrm{lp}}$	$\Delta^{\mathrm{R}}_{\mathrm{lp}}$	$\mathrm{Sel}_{\mathrm{lp}}$
Llama L16/name (clean-strong; positive control)			
T0 (in-distribution)	-1.153	-0.0003	3791
T1	-1.155	-0.0004	3261
T2	-1.337	-0.0004	3266
T3	-1.346	-0.0004	3549
T4	-1.078	-0.0007	1449
T5 (Korean)	-1.135	$+0.0006$	1928
T6	-1.047	-0.0007	1492
T7 (JSON)	-0.669	-0.0016	423
T8 (narrative)	-0.621	-0.0009	692
Gemma L20/name (Failure mode A)			
T0	-2.528	-7.548	0.34
T1	-2.509	-6.787	0.37
T2	-2.415	-7.450	0.32
T3	-2.376	-7.378	0.32
T4	-3.042	-7.046	0.43
T5 (Korean)	-3.459	-7.668	0.45
T6	-2.760	-7.795	0.35
T7 (JSON)	-3.152	-7.134	0.44
T8 (narrative)	-3.002	-8.908	0.34
Llama L8/name (Failure mode B)			
T0	-4.552	-1.925	2.37
T1	-4.565	-1.939	2.35
T2	-4.337	-2.094	2.07
T3	-4.592	-1.850	2.48
T4	-4.415	-2.730	1.62
T5 (Korean)	-4.550	-2.075	2.19
T6	-4.349	-2.217	1.96
T7 (JSON)	-5.606	$+0.269$	20.81
T8 (narrative)	-4.119	-3.144	1.31

Table 9: Per-template results for cells discussed in the main text. T0 retains the original training format containing all four PII fields; T1–T8 isolate a single PII field with varying label formats. Llama L16/name maintains $\mathrm{Sel}_{\mathrm{lp}} > 400$ across all 9 templates including OOD Korean and JSON formats. Gemma L20/name shows $\mathrm{Sel}_{\mathrm{lp}} < 1$ across all 9 templates (Failure mode A).

Model	Layer	name	id	phone	email
Full feature-selection collapse					
Gemma	20	20385	20385	20385	20385
Llama	8	16363	16363	16363	16363
Qwen	9	30639	30639	30639	30639
Partial feature sharing					
Gemma	9	5559	5559	4648	11893
Gemma	31	2807	16900	2807	2807
Llama	16	**32619**	6432	10947	10947
Qwen	18	540	21146	21146	21146
No feature sharing					
Llama	24	4823	25245	5682	26877
Qwen	27	27259	10595	17828	5037

Table 10: Selected feature ID per (model, layer, PII type). Group definitions: *Full collapse*=single selected feature across all 4 PII types; *Partial sharing*=some PII types share a selected feature; *No sharing*=distinct selected feature for all 4 PII types. SAE dictionary size: $d_{\mathrm{sae}} = 28{,}672$ for Gemma, $32{,}768$ for Llama and Qwen. **Bolded**: feature 32619 (Llama L16/name) corresponds to the only clean-strong configuration in the entire grid.

Collapse cell	name	id	phone	email
Gemma L20 (f=20385)	-2.80	-0.47	-0.45	-0.31
Llama L8 (f=16363)	-4.57	-1.96	-1.95	-1.97
Qwen L9 (f=30639)	-1.92	$+0.16$	-0.48	$+1.11$

Table 11: $\Delta^{\mathrm{target}}_{lp}$ per PII type in the three full-collapse cells. Negative values indicate suppression; positive values indicate anti-suppression. Despite shared feature selection and matched activation magnitudes, intervention effects are markedly type-asymmetric: Gemma L20 favors name (6.0× average of others), Llama L8 favors name (2.3×), and Qwen L9 produces anti-suppression for id and email.

not artifacts of this choice, we sweep $\alpha \in \{-1, -2, -3, -4, -5\}$ on three cells representing distinct categories: Llama L16/name (clean-strong), Gemma L20/name (Failure mode A), and Qwen L18/name (clean-weak). All other settings (model, layer, feature, validation pairs) are fixed; templates are restricted to T1 and T5 (one in-distribution, one Korean OOD). The $\alpha = -2$ values match the corresponding 9-template means in Table 8 exactly.

Figure 3 shows that both the clean-strong classification (Llama L16/name) and Failure mode A (Gemma L20/name) are α-robust: selected-feature dominance and random-direction dominance, respectively, hold across all tested α, including the over-perturbation regime at $\alpha = -5$.

Table 14 additionally examines Qwen L18/name as a transitional case: sel_{lp} exceeds 1 at $\alpha = -1, -2$ but flips below 1 from $\alpha = -3$ onward. This indicates that the weak selectivity observed in the main experiment is itself α-dependent, and that $\alpha = -2$ if anything overestimates rather than underestimates selectivity for such cells.

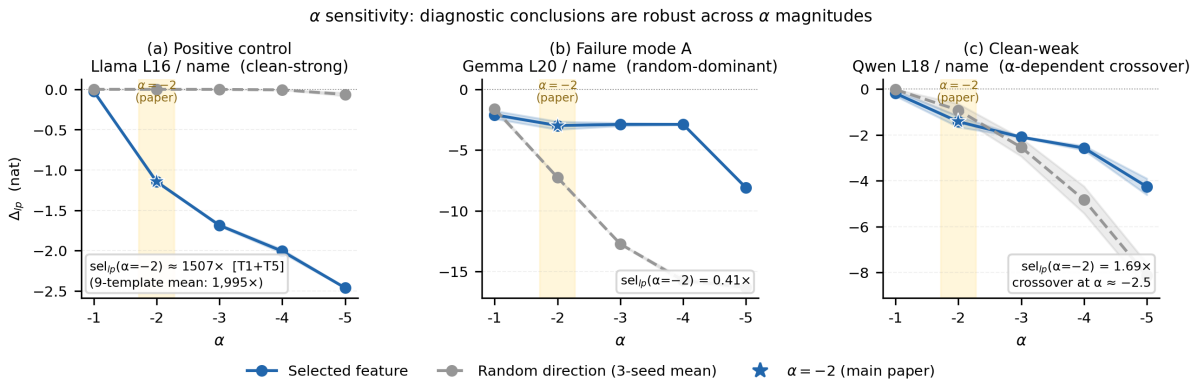

Figure 3: α sensitivity on three representative cells. Yellow band: main-paper setting ($\alpha = -2$). (a) Llama L16/name (clean-strong): selected-feature dominance is preserved across all tested α. (b) Gemma L20/name (Failure mode A): random-direction dominance is preserved across all α, including the over-perturbation regime at $\alpha = -5$. (c) Qwen L18/name (clean-weak): sel_{lp} exceeds 1 at $\alpha = -1, -2$ but crosses below 1 from $\alpha = -3$ onward, indicating that the weak selectivity observed in the main experiment is itself α-dependent.

Threshold	Single-metric	Dual-metric
≥ 2	3 (8.3%)	3 (8.3%)
≥ 3	2 (5.6%)	2 (5.6%)
≥ 5	2 (5.6%)	1 (2.8%)
≥ 10	2 (5.6%)	1 (2.8%)

Table 12: Selectivity threshold sensitivity. Single-metric: $\mathrm{Sel}_{\mathrm{lp}}$ only; Dual-metric: both $\mathrm{Sel}_{\mathrm{lp}}$ and $\mathrm{Sel}_{\mathrm{br}}$ above threshold. Default magnitude gates ($\Delta_{\mathrm{lp}} \leq -0.3$, $\Delta_{\mathrm{br}} \geq +1.0$) and anti-suppression filter retained. Single-metric at ≥ 5 retains Llama L8/phone ($\mathrm{Sel}_{\mathrm{lp}} = 11.2$, $\mathrm{Sel}_{\mathrm{br}} = 3.4$), which dual-metric filters out.

$\lvert\Delta^{\mathrm{T}}_{\mathrm{lp}}\rvert$ gate	$\Delta^{\mathrm{T}}_{\mathrm{br}}$ gate	Cells / 36
≥ 0.0	≥ 0.0	2
≥ 0.0	≥ 0.5	1
≥ 0.3	≥ 1.0 (default)	1
≥ 0.5	≥ 1.0	1

Table 13: Magnitude gate sensitivity at fixed $\mathrm{Sel} \geq 5$. Even the loosest gates yield only 2/36 (5.6%) clean-strong cells.

sel_{lp} as a function of α (T1+T5)					
Cell	-1	-2	-3	-4	-5
Llama L16/name	—	1507	2486	320	39
Gemma L20/name	1.31	0.41	0.23	0.18	0.50
Qwen L18/name	1.31	1.54	**0.83**	0.53	0.52

Table 14: Selectivity ratio sel_{lp} across α for three representative cells: Llama L16/name (clean-strong), Gemma L20/name (Failure A), Qwen L18/name (transitional). Bold marks the α at which selectivity flips below 1. Llama L16/name $\alpha = -1$ omitted ($\lvert\Delta^{\mathrm{random}}_{lp}\rvert$ at measurement floor).